Condition Monitoring of Helicopter Drivetrain Components Using Bispectral Analysis

Mohammed A. Hassan
hassanm@cec.sc.edu
Postdoctoral Researcher
CBM research center
University of South Carolina
Columbia, SC, USA

David Coats
coats@email.sc.edu
Graduate Research Assistant
CBM research center
University of South Carolina
Columbia, SC, USA

Abdel E. Bayoumi
bayoumi@sc.edu
Professor, Director
CBM research center
University of South Carolina
Columbia, SC, USA

ABSTRACT

In this paper, bispectral analysis of vibration signals is used to assess health conditions of different rotating-components in an AH-64D helicopter tail rotor drive train. First, cross-bispectral analysis is used to investigate drive-shaft faulted conditions -- namely misalignment, imbalance, and a combination of misalignment and imbalance -- with respect to a baseline case. The magnitude of the cross-bispectrum shows high sensitivity to abnormalities in the drive shaft, and phase information can be used to distinguish between different shaft conditions. Auto-bispectral analysis is used to study vibration signals collected from a faulted hanger bearing with simultaneous drive shaft misalignment and imbalance. In the presence of drive-shaft faults, shaft harmonics dominate the power spectrum of the vibration signals, making it hard to detect the bearing's fault using only the power spectrum. Application of bispectral analysis provides information about the fault's characteristic frequency and relates spectral contents in the vibration to their physical root causes.

INTRODUCTION

Over the past decade, great advancements have been made in the field of Condition-Based Maintenance (CBM) for aircraft systems [1]-[3]. The successes to date in implementing CBM practices on military helicopters have resulted in the large-scale deployment of Health and Usage Monitoring Systems (HUMS), which have generated a number of benefits ranging from an increased sense of safety to reduced maintenance costs [4]-[6]. To avoid unexpected failure of critical rotorcraft components, on-board HUMS devices continuously collect and process a variety of time-varying waveforms to assess the health conditions of a component. Nevertheless, vibration signals are the most common waveform data used in the condition monitoring of rotating and reciprocating machineries [7]. Collected vibration data are analyzed using different signal processing techniques to extract features that are used to diagnose the current condition of a component, or to estimate its remaining useful life using prognostic models.

Power spectral analysis is the most common technique used in the field of vibration monitoring [8]. The power spectrum describes how the mean square power in a signal is distributed over the frequency. A faulted mechanical component can be detected and isolated when high vibration energy is observed around the characterizing frequency of that component.

However, power spectral analysis has limited performance in describing frequency correlations higher than the second order [9]. The power spectrum is the Fourier transform of the well-known correlation function (second-order moment of the signal) as described by Wiener-Khinchin theorem [10]. Studying higher-order correlation functions and their corresponding spectra could provide more information about the mechanical system, which in turn could help in building more accurate diagnostic models. This information comes with no additional cost in terms of adding more hardware (sensors, wiring, etc.), since further processing of the same collected vibration data is all that is needed. For example, when two faults produce similar characterizing power spectra, such as the case of shaft misalignment and imbalance, further processing of the same vibration data will result in a proper diagnosis of the faults. Another example is when two faults with different characterizing frequencies occur simultaneously such that one fault frequency dominates the power spectrum and masks that of the other fault.

The bispectrum is the Fourier transform of the bicorrelation function (third-order moment), as will be discussed in the following section. It is a very useful tool for investigating quadratic coupling between spectral components [11]. When the system under study has some form of quadratic nonlinearity, various frequency components tend to interact with one another. This frequency mix produces new spectral components which are phase-coupled to the permanent interacting ones. The

Presented at the AHS 70th Annual Forum, Montréal, Québec, Canada, May 20–22, 2014. Copyright © 2014 by the American Helicopter Society International, Inc. All rights reserved.

bispectrum describes the correlation between the source and the result of quadratic-frequency interaction in bi-frequency space.

In this paper, different signal processing techniques based on vibration bispectral analysis are used to assess health conditions of rotating-components in the tail rotor drive train of an AH-64D helicopter. First, different drive-shaft faulted conditions, namely misalignment and imbalance, are investigated using cross-bispectral analysis. Two vibration signals are simultaneously collected from the bearings that support the shafts, then used to estimate the cross-bispectrum and compare it to the classical cross-power spectrum in each case. Condition indicators (CIs) based on magnitude of the cross-bispectrum show higher sensitivity to faults in the studied shaft cases than currently used CIs based on the power spectrum. Also, phase values of the CIs show wider margins between different studied shaft cases, which makes it easy to distinguish each case. Another useful application of the bispectrum is presented to study faulted inner-race of a hanger bearing in the presence of shaft misalignment and imbalance. Analysis of vibration signals from the faulted bearing shows that shaft harmonics dominate the power spectra, making it hard to detect the bearing's fault. Also, unexpected frequencies appear in the vibration spectrum which cannot be explained using conventional power spectral analysis. However, using the auto-bispectral analysis demonstrates better capability in both detecting the fault frequency and relating frequencies in the power spectrum to their physical root causes.

The paper is organized as follows: First, the background of bispectral analysis is sketched. Then, the experimental test stand used to conduct this study is described. Two case studies are presented to demonstrate the applications of bispectrum. These are followed by some concluding remarks.

BISPECTRUM BACKGROUND

Vibration signals collected from rotating mechanical components can be considered as realizations of random processes. Just as random variables are characterized by certain expected values (or, moments), such as mean and variance, random processes are also characterized by their mean value, correlation function, and various higher-order correlation functions. Alternatively, random processes may be characterized by the Fourier transforms of the various order correlation functions [11]. Of particular interest are the correlation and bicorrelation functions and their Fourier transform, as will be discussed in the following subsections.

Auto- and Cross-Power Spectra

For a zero-mean stationary vibration signal $x(t)$, the autocorrelation function $R_{xx}(\tau)$ and the auto-power spectrum $P_{XX}(f)$ are Fourier transform pairs according to the Wiener-Khinchin theorem [10], and can be estimated by equations (1) and (2) as follows:

$$R_{xx}(\tau) = E\{x(t+\tau)x^*(t)\} \tag{1}$$

$$P_{XX}(f) = E\{X(f)X^*(f)\} = E\{|X(f)|^2\} \tag{2}$$

where $E\{.\}$ denotes a statistical expected value operator, $X(f)$ is the Fourier transform of $x(t)$, and superscript asterisk * denotes a complex conjugate.

Auto-power spectrum, $P_{XX}(f)$, is one of the most commonly used tools in vibration spectral analysis [8]. It describes how the mean square power of the vibration signal is distributed over single-frequency space. When two vibration signals are collected simultaneously, cross-correlation, $R_{xy}(\tau)$, is a useful function which investigates the linear relationship between the two signals $x(t)$ and $y(t)$, as given in equation (3). The Fourier transform of the cross-correlation function is the cross-power spectrum, $C_{XY}(f)$, as given in equation (4).

$$R_{xy}(\tau) = E\{x(t+\tau)y^*(t)\} \tag{3}$$

$$C_{XY}(f) = E\{X(f)Y^*(f)\} = |C_{xy}(f)|\, e^{j\theta_{XY}} \tag{4}$$

Auto- and Cross-Bispectra

Auto-bispectrum, $S_{XXX}(f_1,f_2)$, is the Fourier transform of the second-order correlation function $R_{xxx}(\tau_1, \tau_2)$, as given in (5) and (6), and it describes second-order statistical dependence between spectral components of signal $x(t)$ [11].

$$R_{xxx}(\tau_1,\tau_2) = E\{x(t+\tau_1)x(t+\tau_2)x^*(t)\} \tag{5}$$

$$S_{XXX}(f_1,f_2) = E\{X(f_1)X(f_2)X^*(f_1+f_2)\} \tag{6}$$

The advantage of bispectral over power spectral analysis is its ability to characterize quadratic nonlinearities in monitored systems. Due to quadratic nonlinearities, various spectral components of the vibration signal interact with one another producing cross-term (second-order term), as indicated in the left side of equation (7). This interaction results in new combinations of frequencies at both the sum and the difference values of the interacting frequencies, as indicated in the right side of equation (7). An important signature for detecting nonlinearity is based on the knowledge that phase coherence (phase coupling) exists between the primary interacting frequencies and the resultant new sum and difference frequencies. The bispectrum describes this correlation between the three waves (the interacting frequencies i) f_1 and ii) f_2, and the result iii) (f_1+f_2) of nonlinear process) in two-dimensional frequency space (f_1-f_2). The definition of the bispectrum in (6) implies that $S_{XXX}(f_1,f_2)$ will be zero unless phase coherence is present between the three frequency components f_1, f_2, and $f_1 + f_2$.

$$\begin{aligned}\cos(2\pi f_1 t+\theta_1)\times\cos(2\pi f_2 t+\theta_2) \\ = \frac{1}{2}[\cos(2\pi(f_1+f_2)t+(\theta_1+\theta_2)) \\ +\cos(2\pi(f_1-f_2)t+(\theta_1-\theta_2))]\end{aligned} \tag{7}$$

Similarly, the cross-bispectrum $C_{XXY}(f_1,f_2)$ is the Fourier transform of the cross-bicorrelation function $R_{xxy}(\tau_1,\tau_2)$ as given in (8) and (9) [11]:

$$R_{xxy}(\tau_1,\tau_2) = E\{x(t+\tau_1)x(t+\tau_2)y^*(t)\} \quad (8)$$

$$C_{XXY}(f_1,f_2) = E\{X(f_1)X(f_2)Y^*(f_1+f_2)\} \quad (9)$$

The cross-bispectrum given in (9) investigates the nonlinear coupling between any two frequency components f_1 and f_2 in signal $X(f)$ that interact, due to quadratic nonlinearity, to produce a third frequency f_1+f_2 at another signal $Y(f)$.

Both auto- and cross-bispectrum will be evaluated digitally. Sampling theory implies that f_1, f_2, and $f_3=f_1+f_2$ must be less than or equal to $(f_S/2)$, where f_S is the sampling frequency. Due to sampling theory limitations in addition to Fourier transform symmetry properties, cross-bispectrum, $C_{XXY}(f_1,f_2)$, is usually plotted in the sum-frequency region denoted by "Σ" and the difference-frequency region "Δ", as shown in Figure 1, while auto- bispectrum, $S_{XXX}(f_1,f_2)$, is usually plotted only in the sum-frequency region "Δ" [11].

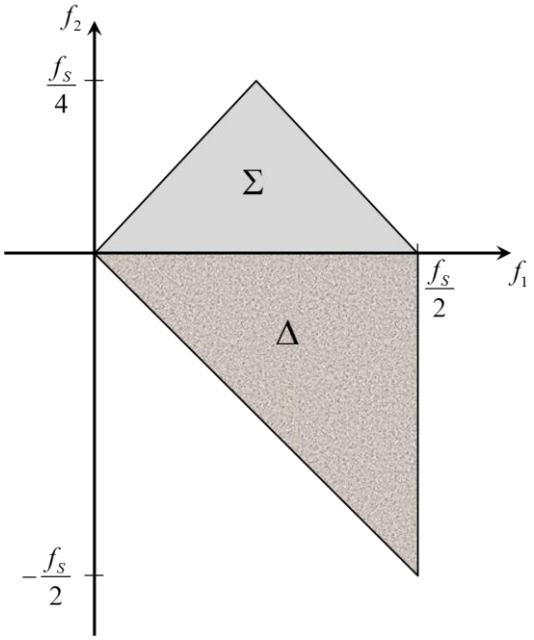

Figure 1: Region of computation of the bispectrum

TRDT TEST STAND AT USC

Since 1998, the University of South Carolina (USC) has been working closely with the South Carolina Army National Guard on a number of projects directed at reducing the Army's aviation costs and at increasing its operational readiness through the implementation of CBM [5]-[6]. These efforts expanded into a fully-matured CBM research center which hosts several aircraft component test stands in support of current US Army CBM objectives [2]. Within the USC test facility is an AH-64D (Apache helicopter) tail rotor drive train (TRDT) test stand for on-site data collection and analysis, as shown in Figure 2-(b).

The TRDT test stand emulates the complete tail rotor drive train from the main transmission tail rotor power takeoff to the tail rotor swashplate assembly, as shown in Figure 2-(a). This multi-shaft drive train consists of four shafts. Three of these shafts, denoted as shafts #3, #4 and # 5, lead from the tail rotor power take off point to the intermediate gearbox (IGB). These shafts are supported by two hanger bearings denoted as forward (FHB) and aft (AHB), and flexible couplings at shaft joining points. The fourth shaft is installed on the vertical stabilizer between the IGB and the tail rotor gearbox (TRGB).

All drive train parts on the test stand are actual aircraft hardware. The prime mover for the drive train is an 800hp AC induction motor controlled by a variable-frequency drive. An absorption motor of matching rating, controlled by a separate variable-frequency drive, is used to simulate the torque loads that would be applied by the tail rotor. The input and the output motors work in dynamometric configuration to save energy.

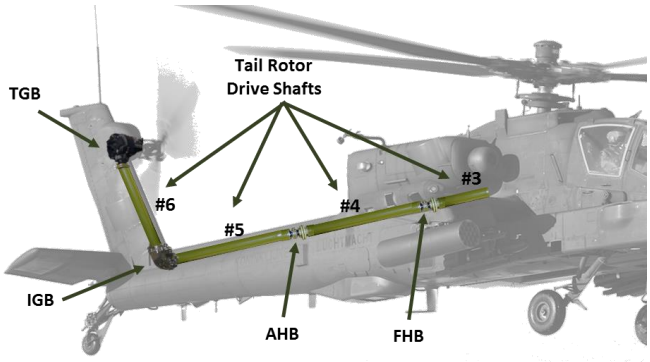

(a) TRDT on the AH-64D helicopter

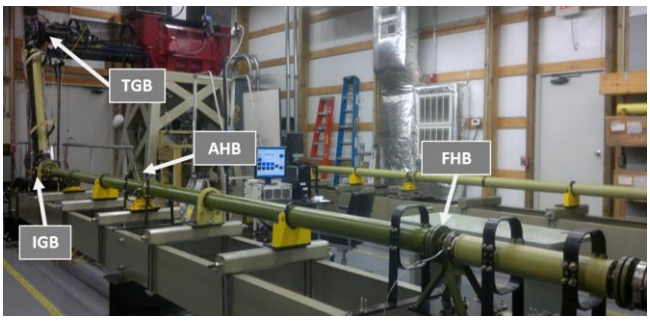

(b) TRDT test stand at USC

Figure 2: Tail Rotor Drive Train (TRDT)

The structure, instrumentation, data acquisition systems, and supporting hardware are in accordance with military standards. The signals being collected during the operational run of the stand include vibration data measured by accelerometers, temperature measured via thermocouples, and speed and torque measurements. The measurement

devices are placed at the FHB and AHB hanger bearings and the two gearboxes as shown in Figure 2-(b).

DRIVE-SHAFT CASE STUDY

In this section, we utilize the cross-bispectrum as a tool to investigate and model quadratic nonlinear relationships between two vibration signals simultaneously collected at the FHB and AHB positions in an AH-64D helicopter tail rotor drive train.

Experiment Setup and Vibration Data Description

The data used in this study were collected from four experiment runs testing different shaft alignment and balance conditions. In order to keep data organized, a naming convention, summarized in Table 1, was adopted. The original configuration of the test stand used balanced drive-shafts, straightly aligned, as a baseline for normal operations (case "00373" in Table 1). The case of aligned but unbalanced shafts ("10373" in Table 1) is simulated with drive shaft #4 unbalanced by 0.135 oz-in, and drive shaft #5 unbalanced by 0.190 oz-in. Angular misalignment between shafts (case "20373" in Table 1) was tested with a 1.3 misalignment between the #3 and the #4 drive shafts and a similar misalignment between the #4 and the #5 drive shafts. A combination of the last two cases, imbalance and misalignment, was also tested (case "30373" in Table 1).

Table 1. Vibration Data Set and Test Numbers

Shaft Setting	Test Number
Baseline (Aligned-Balanced) (BL)	00373
Aligned-Unbalanced (UB)	10373
Misaligned-Balanced (MA)	20373
Misaligned-Unbalanced (MA-UB)	30373

During each thirty-minute run, accelerometer data were collected simultaneously from the FHB and AHB once every two minutes, making total of 15 data samples. Each data sample consists of 65536 data points collected at a sampling rate of 48 kHz (f_S), which results in a data collection time of approximately 1.31 seconds per acquisition. Vibration signals are collected during operation of the test stand at a constant rotational speed of 4863 rpm (81.05 Hz), with a simulation of the output torque at 111 ft-lb. Rotational speed is the speed of the input shafts and hanger bearings. Output torque is given by the torque at the output of the tail rotor gearbox simulating rotor operation while the torque applied to the input shafts is equal to 32.35 ft-lb.

Results and Discussion

Vibration signals at the FHB and AHB in Figure 2 are used as *x(t)* and *y(t)* in equations (4) and (9). In the following discussion, for easier notation of frequency values, we will use "1R, 2R, 3R, etc." to denote "first, second, third, etc." harmonics of the shaft rotating frequency (1R = 81.05Hz).

Figure 3 shows the magnitude plot of the cross-power spectrum for all the studied shaft settings. Although we expect to see very low vibration power in the case of the baseline, Figure 3(a) shows a high spectral peak at *f=3R* that dominates the vibration spectrum in this case. High vibration power at this frequency can be caused by oscillations due to unsymmetrical loading on one end of the drive shafts as torque transferred to the shafts through the IGB from the tail rotor. A high spectral peak at frequency 3R continues to dominate all the studied faulted cases, as shown in Figure 3(b-d).

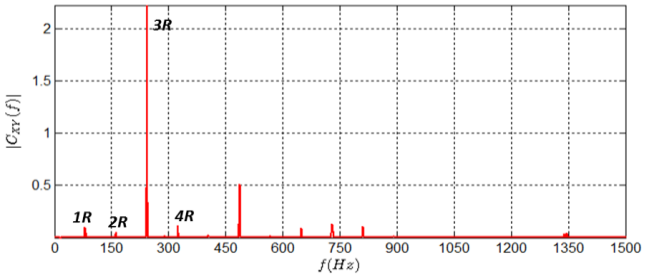

(a) Baseline case (00373)

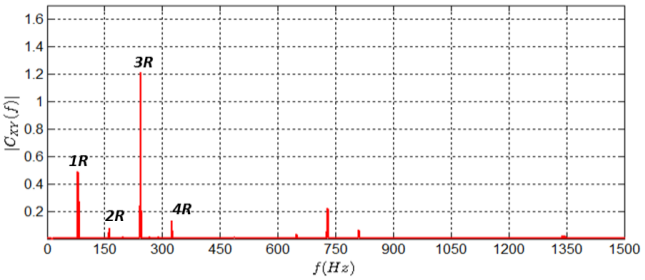

(b) Unbalanced case (10373)

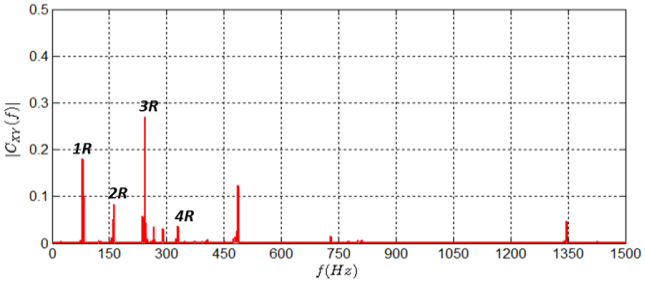

(c) Misaligned case (20373)

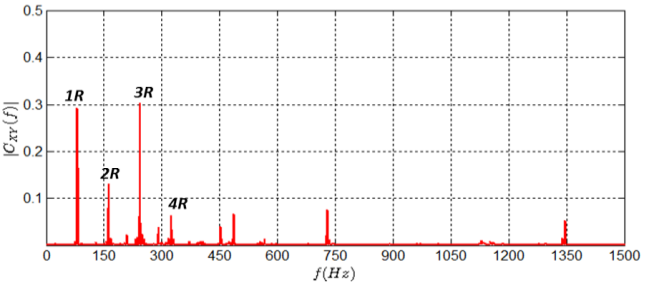

(d) Misaligned-Unbalanced case (30373)

Figure 3. Cross-power spectrum between FHB and AHB vibration signals under different shaft settings

Current practice in monitoring rotating shaft conditions involves using the vibration magnitude at the spectral peaks corresponding to the first three rotating shaft harmonics (1*R*, 2*R*, and 3*R*) as shaft's condition indicators [12], [13]. In order to calculate those condition indicators, either an auto-power spectrum is averaged between the two vibration signals at one particular frequency (for example, 2R) or a cross-power spectrum between the two vibration signals is calculated at that frequency. Comparison with the baseline is usually done on a logarithmic amplitude scale, where increases of 6-8 dB (double the baseline values) are considered to be significant and changes greater than 20 dB (ten times the baseline values) are considered serious [14]. Therefore, we will focus our attention on comparing the experimental data using *1R*, 2*R*, and *3R* condition indicators calculated from the cross-power spectrum between the FHB and AHB vibrations.

Table 2 summarizes the results of the spectral peak comparison of the three faulted cases (UB, MA, and MA-UB) against the baseline case (BL). Values of spectral peaks at the first three harmonics of the shaft speed (*1R, 2R,* and *3R*) are extracted from the cross-power spectral plots in Figure 3(b-d), and compared with their counterparts from the baseline case (Figure 3(a)) in logarithmic scale. Results of the spectral peak comparison in Table 2 show that vibration power at shaft rotation frequency *(f=1R)* exceeds the 6 dB threshold in all the faulted cases, and hence is considered a good indicator of the faults. However, using only the magnitude of *1R* condition indicator does not give much information to distinguish between different studied faults.

Table 2. Spectral Peak Comparison with Baseline (dB)

f	UB(10373)	MA(20373)	MA-UB(30373)
1R	16.22	6.31	11.09
2R	3.51	4.58	9.12
3R	-6.08	-20.89	-19.95

In order to gain more diagnostic capabilities, phase information of the cross-power spectral peaks can be employed. Phase differences between spectral peaks of faulted cases compared to the baseline are listed in Table 3 for the first three harmonics of the rotating shaft frequency (*1R*, *2R*, and *3R*). For the *1R* frequency, whose magnitude is used as a fault indicator, narrow phase margins can be observed between different cases, as shown in Table 3.

Table 3. Cross-Power Phase Comparison with Baseline (Degrees)

f	UB(10373)	MA(20373)	UB-MA(30373)
IR	-35.05	-53.41	-39.97
2R	-19.04	22.69	1.93
3R	7.85	-69.48	-53.34

More information can be extracted from the same vibration data by extending the analysis to investigate the quadratic-nonlinear behavior of the drive shafts using the cross-bispectrum. Magnitude of the cross-bispectrum is plotted for the same data set studied before, as shown in Figures 4. The baseline case (aligned-balanced), shown in Figure 4(a), has the least quadratic nonlinear frequency interaction of all cases. The highest bispectral peak in the baseline case is found at the coordinate point (*3R*,*3R*) whose magnitude is equal to 0.17 g^3. For faulted shaft cases, increased frequency-interaction takes place along f_1=*1R, 2R,* and *3R* frequency axes, as can be observed in Figure 4(b-d). One interesting observation is the high bispectral peaks at the frequency coordinate points of (*1R*,*1R*), (*2R*,*1R*), and (*3R*,*1R*) in all the faulted cases compared to the baseline. Interpretation of these frequency coupling points suggests that quadratic nonlinearity of the faulted drive shafts stimulates interaction between time-varying forces at the shaft rotation frequency, *1R*, and its harmonics.

Bispectral peaks at the three frequency coordinate points mentioned above are used to compare the three faulted cases with the baseline case, as summarized in Table 4. Bispectral peaks at (*1R*,*1R*), (*2R*,*1R*), and (*3R*,*1R*) are extracted from each faulted case and compared to their counterparts from the baseline in logarithmic scale. Results of the bispectral peak comparison in Table 4 show the sensitivity of all the selected bispectral condition indicators to any abnormalities in the drive shafts. Values of those bispectral peaks increase more than 6dB in all the faulted cases compared to the baseline.

Table 4. Bispectral Peak Comparison with Baseline (dB)

(f_1,f_2)	UB(10373)	MA(20373)	MA-UB(30373)
(1R,1R)	16.35	12.92	16.89
(2R, 1R)	10.64	9.44	8.25
(3R,1R)	16.33	8.05	11.93

Again, phase information of the cross-bispectral peaks can be used to gain more diagnostic capabilities. Phase differences are calculated between the bispectral peaks in faulted cases and their counterparts in the baseline, as listed in Table 5. Wider phase margins can be observed between different faulted cases. These wider margins relax the requirement to set threshold values and make it easy to distinguish between different cases.

Table 5. Cross-Bispectrum Phase Comparison with Baseline (Degrees)

(f_1,f_2)	UB(10373)	MA(20373)	MA-UB(30373)
(1R,1R)	-53.53	60.17	-69.60
(2R, 1R)	1.12	-94.16	0.18
(3R,1R)	-117.99	-302.09	71.30

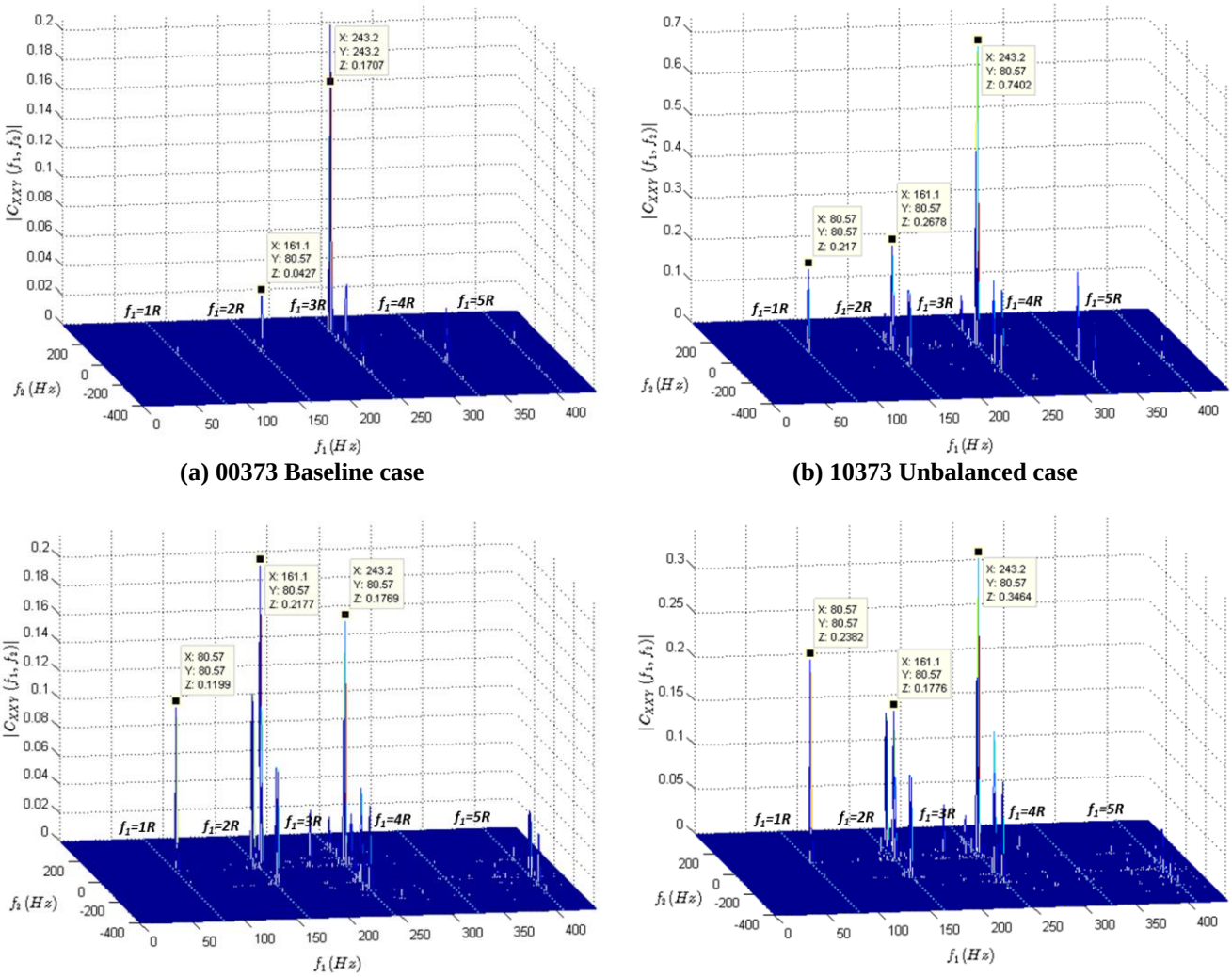

(a) 00373 Baseline case **(b) 10373 Unbalanced case**

(c) 20373 Misaligned case **(d) 30373 Unbalanced-Misaligned case**

Figure 4: Cross-bispectrum between FHB and AHB vibration signals under different shaft settings

BEARING CASE STUDY

Most of the conventional fault analysis techniques assume that a defect occurs in a rotating element separately, that we can identify a fault by the characterizing frequency of that component. For example, ball pass frequency inner-race (BPFI) is used to detect faults in the inner-race of bearings [15]. However, in the presence of drive shaft faults, shaft harmonics dominate the power spectra of the vibration signals collected form the faulted hanger bearing, making it hard to detect bearing faults. Also, spectral interaction between different fault frequencies leads to the appearance of unexpected frequencies in the vibration spectrum which cannot be explained using conventional power spectral analysis.

In this section, the auto-bispectrum is used to analyze vibration data collected from a faulted hanger bearing with typically misaligned and unbalanced shafts.

Experiment Setup and Vibration Data Description

A seeded hanger bearing fault experiment was designed to test multi-faulted drive train components. The FHB was machined to replicate a bearing with a spalled inner-race, as shown in Figure 5. The faulted hanger bearing was tested with 1.3° misalignment between drive shafts #3 and #4, 1.3° misalignment between drive shafts #4 and #5, and drive shafts #3, #4, and #5 unbalanced by 0.14 oz-in, 0.135 oz-in, and 0.19 oz-in, respectively.

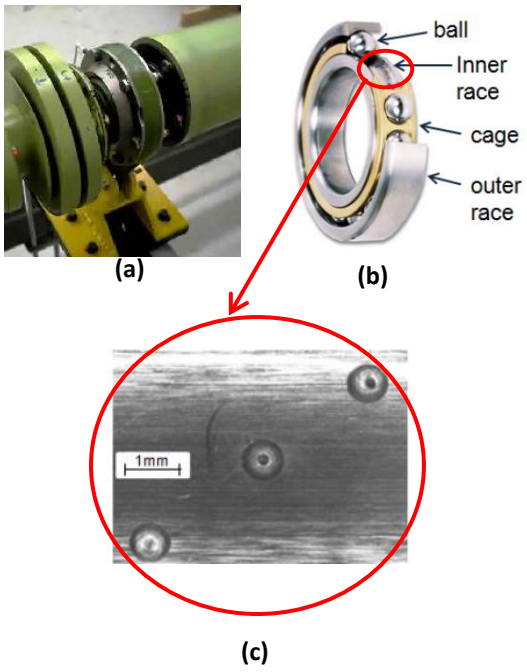

Figure 5: Faulted FHB: (a) assembled bearing in the drive train, (b) schematic of assembly components, and (c) zoom-in view of the spalled inner-race fault

Three holes were milled into the inner-race with a ball mill and were machined to the specifications summarized in Table 6. Vibration data were collected every two minutes over a 50 minutes run. Each acquisition consisted of 65536 data points collected at a sampling rate of 48 kHz (f_S). Vibration signals were collected during operation of the test stand at a constant rotational speed of 4863 rpm (81.05 Hz) from the prime mover, and output torque at the tail rotor equals to 371 ft-lb.

Table 6. Spalled Inner-Race Specifications (inch)

Spall	Diameter	Depth	Distance from left shoulder	Distance from right shoulder
#1	0.031	0.017	0.1400	0.2538
#2	0.031	0.016	0.1956	0.1985
#3	0.031	0.017	0.2567	0.1376

Results and Discussion

Magnitude of the auto-power spectrum for vibration data collected form the spalled inner-race FHB is shown in Figure 6. Due to the presence of the drive shafts misalignment and imbalance, high magnitudes of the vibration exist at the 80.57Hz, 162.5Hz, and 243.2Hz. These frequencies match *1R* , *2R*, and *3R*, and indicate drive shaft faults as discussed in the previous section. Due to the presence of the fault in the inner-race of the bearing, one should also expect to see the ball pass inner-race frequency (BPFI) that characterizes the faulted hanger bearing under test (441Hz as reported by the Aviation Engineering Directorate (AED)). However, vibration power at PBFI has very low magnitude, making it very hard to detect, as shown in Figure 6. The highest non-shaft frequency in this spectrum is at 684.1Hz, which does not match any frequency reported by AED for the tail rotor drive train components.

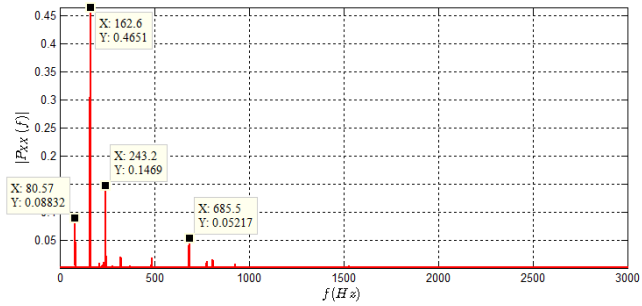

Figure 6: Power spectrum of the spalled inner-race FHB with misaligned-unbalanced shafts

Auto-bispectrum is utilized to investigate the same vibration data from the faulted inner-race bearing, as shown in Figure 7. It can be seen that a number of quadratic frequency interactions exist along the first three shaft rotating harmonics (f_1 = 80.57Hz, 161.1Hz, and 243.2Hz). These shaft harmonic patterns have been used before to describe shaft abnormalities. Among frequency interaction pairs, the high bispectral peak at the (442.4Hz, 243.2Hz) coordinate point has very interesting interpretation. First, physical interpretation of this bispectral peak suggests that the 442.4Hz frequency nonlinearly interacts with third harmonic of the shaft, 243.2Hz, to produce the sum value, 684.6Hz. The existence of the 685.6Hz frequency value in the power spectrum of the bearing's vibration could not be explained using information from the power spectrum alone. Also, 442.4Hz is equal to the BPFI, which implies that a fault exists in the inner race of the hanger bearing.

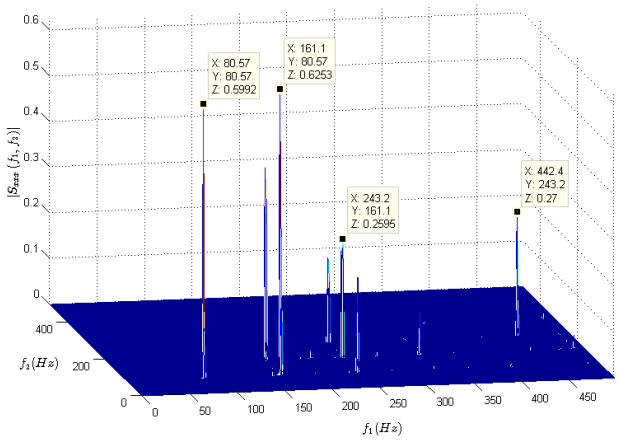

Figure 7: Aut-bispectrum of the spalled inner-race FHB with misaligned-unbalanced shafts

CONCLUSION

In this paper, bispectral analysis has been used to investigate and understand quadratic nonlinear wave-wave interaction in vibration signals in order to assess health conditions of rotating components in the AH-64D helicopter tail rotor drive train. First, cross-bispectrum has been employed to study quadratic coupling in faulted drive shafts. Compared with conventional power spectral analysis, condition indicators based on magnitude of the cross-bispectrum have shown higher sensitivity to abnormalities in the drive shafts. Moreover, phase information from the bispectrum has shown wider phase margins among different studied shaft cases which makes it easy to distinguish between different shaft conditions.

Auto-bispectrum has also been used to study vibration signals from a faulted hanger bearing under simultaneous drive shaft misalignment and imbalance. In the presence of the drive-shaft faults, shaft harmonics have dominated the power spectra of the vibration signals collected from the faulted hanger-bearing, making it hard to detect the bearing's fault. Also, unexpected frequencies have appeared in the vibration spectra which could not be explained using conventional power spectral analysis. However, bispectral analysis has not only detected the bearing's fault, but also has shown better ability to relate all frequencies in the power spectrum to their root causes and successfully link the signal processing to the physics of the underlying faults.

Future research in this area includes studying the effect of loading by the trail-rotor blades on the proposed metrics, and extending the application of bispectral analysis to study more faults and failure modes in aircraft. The unique quadratic nonlinearity signature of each fault can be used to design more accurate and reliable diagnostic algorithms for condition-based maintenance (CBM) practice.

ACKNOWLEDGMENT

This research was funded by the South Carolina Army National Guard and United States Army Aviation and Missile Command via the Conditioned-Based Maintenance (CBM) Research Center at the University of South Carolina-Columbia.

REFERENCES

[1] A. K.S. Jardine, D. Lin, and D. Banjevic, "A Review on Machinery Diagnostics and Prognostics Implementing Condition-Based Maintenance," Mechanical Systems and Signal Processing, vol. 20, no. 7, pp. 1483-1510, Oct. 2006.

[2] V. Blechertas, A. Bayoumi, N. Goodman, R. Shah, and Yong-June Shin, "CBM Fundamental Research at The University of South Carolina: A Systematic Approach to U.S. Army Rotorcraft CBM and the Resulting Tangible Benefits," Presented at the American Helicopter Society Technical Specialist Meeting on Condition Based Maintenance, Huntsville, AL, USA, pp. 1-20, Feb. 2009.

[3] M. A. Hassan, D. Coats, Yong-June Shin, and A. Bayoumi, "Quadratic-Nonlinearity Power-Index Spectrum and Its Application in Condition Based Maintenance (CBM) of Helicopter Drive Trains," Proceeding of the IEEE International Instrumentation and Measurement Technology Conference (I2MTC), pp. 1456-1460, May 2012.

[4] P. Grabill, T. Brotherton, J. Berry, and L. Grant, "The US Army and National Guard Vibration Management Enhancement Program (VMEP): Data Analysis and Statistical Results," American Helicopter Society 58th Annual Forum, Montreal, Cananda, June, 2002.

[5] A. Bayoumi, W. Ranson, L. Eisner, and L.E. Grant, "Cost and effectiveness analysis of the AH-64 and UH-60 on-board vibrations monitoring system," IEEE Aerospace Conference, pp. 3921-3940, Mar. 2005.

[6] A. Bayoumi, and L. Eisner, "Transforming the US Army through the Implementation of Condition-Based Maintenance," Journal of Army Aviation, May 2007.

[7] P. D. Samuel, and D. J. Pines, "A Review of Vibration-Based Techniques for Helicopter Transmission Diagnostics," Journal of Sound and Vibration, vol. 282, no. 1-2, pp. 475-508, Apr. 2005.

[8] A. S. Sait, and Y. I. Sharaf-Eldeen, "A Review of Gearbox Condition Monitoring Based on Vibration Analysis Techniques Diagnostics and Prognostics," in Rotating Machinery, Structural Health Monitoring, Shock and Vibration, Vol. 8, T. Proulx, Ed. New York: Springer, pp. 307- 324, 2011.

[9] M. A. Hassan, A. E. Bayoumi, and Y.-J. Shin "Quadratic-Nonlinearity Index Based on Bicoherence and Its Application in Condition Monitoring of Drive-Train Components," IEEE Transactions on Instrumentation and Measurement, vol. 63, no. 3, pp. 719-728, March 2014.

[10] John G. Proakis, and Dimitris G. Manolakis, "Power Spectrum Estimation," in Digital Signal Proccessing: Principles, Algorithms, and Applications, 4th ed. New Jersey: Prentice Hall, 2007, pp. 960-1040.

[11] B. Boashash, E. J. Powers, A. M. Zoubir, "Higher-Order Statistical Signal Processing," Wiley, 1996.

[12] Damian Carr. "AH-64A/D Conditioned Based Maintenance (CBM) Component Inspection and Maintenance Manual Using the Modernized Signal Processor Unit (MSPU) or VMU (Vibration Management Unit)," Aviation Engineering Directorate Apache Systems, Alabama, Tech. Rep., Oct. 2010.

[13] P. Grabill, J. Seale, D. Wroblewski, and T. Brotherton, "iTEDS: the intelligent Turbine Engine Diagnostic System," Proceedings of 48 International Instrumentation Symposium, May 2002.

[14] R. B. Randall, "Fault Detection," in Vibration-based Condition Monitoring: Industrial, Aerospace and Automotive Applications, Wiley, 2011.

[15] C. Scheffer, P. Girdhar, "Practical Machinery Vibration Analysis and Predictive Maintenance," 2004.